



Crystal structure effect on the phase transition of $(\text{Ca}_{0.28}\text{Ba}_{0.72})_x(\text{Sr}_{0.61}\text{Ba}_{0.39})_{1-x}\text{Nb}_2\text{O}_6$ ceramics

Yu Xu¹ · Hongbo Liu¹

Received: 4 January 2020 / Accepted: 10 February 2020 / Published online: 17 February 2020
© Springer Science+Business Media, LLC, part of Springer Nature 2020

Abstract

$(\text{Ca}_{0.28}\text{Ba}_{0.72})_x(\text{Sr}_{0.61}\text{Ba}_{0.39})_{1-x}\text{Nb}_2\text{O}_6$ ceramics have been prepared by a solid-state reaction method. With the increase of x , the nature of the phase transition varies from the diffuse to the normal, and the phase transition temperature increases. The structural origins of these variations were studied by Rietveld refinement and Raman spectroscopy. The results indicate that the change of the phase transition type is related to the site-occupancy factors of cations at A sites and the increased phase transition temperature is because of the enhanced structural deformation of oxygen octahedral. This enhanced ferroelectricity makes the system have potential applications for high-temperature environments.

1 Introduction

Tetragonal tungsten bronze (TTB) oxides are very important electronic materials for a variety of applications due to their excellent piezoelectric, pyroelectric, optical properties [1–4]. Figure 1 shows the crystal structure of unfilled TTB viewing along the c axis. In one lattice, ten distorted octahedrons share corners and three different interstices (two A1, four A2, and four C) are available for cations. Thus, the general formula of TTB is $(\text{A}1)_2(\text{A}2)_4\text{C}_4(\text{B}1)_2(\text{B}2)_8\text{O}_{30}$. The size of A2 is larger than that of A1, and one of A sites and all C sites are empty for unfilled TTB.

In unfilled TTB, $(\text{Sr}_{0.61}\text{Ba}_{0.39})\text{Nb}_2\text{O}_6$ is the most studied one and has been applied in electro-optic devices. However, the phase transition temperature of $(\text{Sr}_{0.61}\text{Ba}_{0.39})\text{Nb}_2\text{O}_6$ is low, which limits its applications at high temperatures. T_m at which the dielectric permittivity gets a maximum varies from 66 to 89 °C [3, 5–7]. Another commonly studied TTB is $(\text{Ca}_{0.28}\text{Ba}_{0.72})\text{Nb}_2\text{O}_6$ [8, 9], which has high-phase transition temperature at 252–327 °C [8, 10–12]. It is, therefore, interesting to prepare the solid solution ceramics $(\text{Ca}_{0.28}\text{Ba}_{0.72})_x(\text{Sr}_{0.61}\text{Ba}_{0.39})_{1-x}\text{Nb}_2\text{O}_6$, since preparing solid solution is one of the main methods to enhance the functionality of electronic materials [13–15]. In addition, there are three cations (Ca^{2+} , Sr^{2+} , and Ba^{2+}) with

different radii occupying A1/A2 sites in the solid solution of $(\text{Ca}_{0.28}\text{Ba}_{0.72})_x(\text{Sr}_{0.61}\text{Ba}_{0.39})_{1-x}\text{Nb}_2\text{O}_6$. The site occupancies of these cations are the additional freedoms to modify the functional properties of the unfilled TTB oxides.

Recently, the dielectric properties of the single crystals of $(\text{Ca}_{0.28}\text{Ba}_{0.72})_x(\text{Sr}_{0.61}\text{Ba}_{0.39})_{1-x}\text{Nb}_2\text{O}_6$ were reported [16]. However, there is no result on the properties of the ceramics of $(\text{Ca}_{0.28}\text{Ba}_{0.72})_x(\text{Sr}_{0.61}\text{Ba}_{0.39})_{1-x}\text{Nb}_2\text{O}_6$. In this work, the ceramics of $(\text{Ca}_{0.28}\text{Ba}_{0.72})_x(\text{Sr}_{0.61}\text{Ba}_{0.39})_{1-x}\text{Nb}_2\text{O}_6$ were prepared using the solid reaction method. The structural, dielectric, and ferroelectric properties of the ceramics were studied in detail. The phase transition varies from the diffuse to the normal with the increase of x , which is discussed with the site-occupancy factors of Ca^{2+} , Sr^{2+} , and Ba^{2+} at A1/A2 sites of the TTB structure. With the increase of x , the phase transition temperature also increases. This is related to the enhanced oxygen octahedral distortion. High phase transition temperature makes the ceramics useful in high-temperature electronic devices.

2 Experimental details

The ceramics with the composition $(\text{Ca}_{0.28}\text{Ba}_{0.72})_x(\text{Sr}_{0.61}\text{Ba}_{0.39})_{1-x}\text{Nb}_2\text{O}_6$ ($x = 0.25, 0.5, \text{ and } 0.75$) (abbreviated as CSBN25, CSBN50, and CSBN75, respectively) were synthesized by the conventional solid-state reaction method with the high purity raw materials of Nb_2O_5 (99.9%), SrO (99.9%), BaCO_3 (99.9%) and CaCO_3 (99.9%). The weighed raw materials were ball-milled for

✉ Hongbo Liu
bohongliu@gmail.com

¹ School of Materials Engineering, Shanghai University of Engineering Science, Shanghai 201620, China

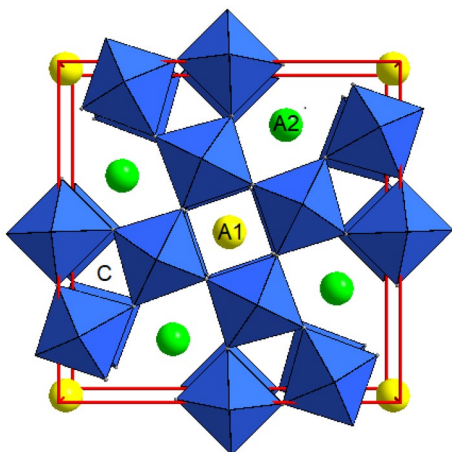


Fig. 1 The crystal structure of unfilled TTB viewing along the *c*-axis

10 h with ethanol, calcinated in a furnace at 1200 °C for 3 h, and then pressed into disc pellets with a diameter of 13 mm and a thickness of 1 mm under a uniaxial press of 300 MPa. The pellets were then sintered at 1200–1300 °C for 3 h. The crystal structures of the ceramics were analyzed using an X-ray diffraction Diffractometer (PANalytical X'Pert PRO). The morphology of the samples was investigated using a scanning electron microscope (TESCAN-VEGA3). The dielectric properties were measured by an impedance analyzer (Keysight E4990A) in the frequency range of 1 kHz–1 MHz. The ferroelectric properties were characterized by a commercial ferroelectric tester (Radiant Technology Precision LC ferroelectric tester). The Raman spectra of the materials were recorded using a Raman spectrometer (Horiba HR Evolution) with laser excitation at 532 nm.

3 Results and discussion

Figure 2 shows the microstructures of the prepared ceramics. All ceramics are dense and without pores. This is consistent with the density characterization that the relative densities are higher than 97% for all ceramics. The average size of ceramics is ca. 1 μm. The grains are homogenous and no pillar grain morphology is observed as in some TTB ceramics [3, 17]. However, the growth spirals are noticed for CSBN50, which indicates an initial partial melting of the grains and the diffusion of ions to the growing steps through the fluid phase [17]. As a result, more defects may induce because the sintering mechanism is related to the screw dislocations. These defects could deteriorate the electrical properties of CSBN50.

Figure 3a–c shows the dielectric permittivity of the ceramics at 1 kHz–1 MHz. The temperature-dependent dielectric permittivity at 1 MHz was fitted by the power law [18, 19]:

$$\frac{\epsilon_m}{\epsilon} = 1 + \frac{(T - T_m)^\gamma}{2\delta_m^2} \quad (1)$$

where γ is the diffuseness exponent of the phase transition. If $\gamma = 1$, the equation equals to Curie–Weiss law; if $\gamma = 2$, it corresponds to a complete diffuse phase transition, the ferroelectric clusters are completely frustrated; the correlated ferroelectric clusters give γ in between 1 and 2. δ_m is the broadening parameter, ϵ_m is the maximum dielectric permittivity and T_m is the corresponding temperature. The fitted γ is 1.25, 1.13, and 1.08 for CSBN25, CSBN50, and CSBN75, respectively. The fitted δ_m is 14.2, 11.1, and 8.7, respectively. They imply that with the increase of x , the phase transition varies from the diffuse to the normal ferroelectric. The fitted T_m is 145, 186, and 279. The increased phase transition temperature is more clearly depicted in Fig. 3d with the dielectric permittivity at 1 MHz. The improved phase transition temperature is very important for the applications of the ceramics at high-temperature. The dielectric permittivity

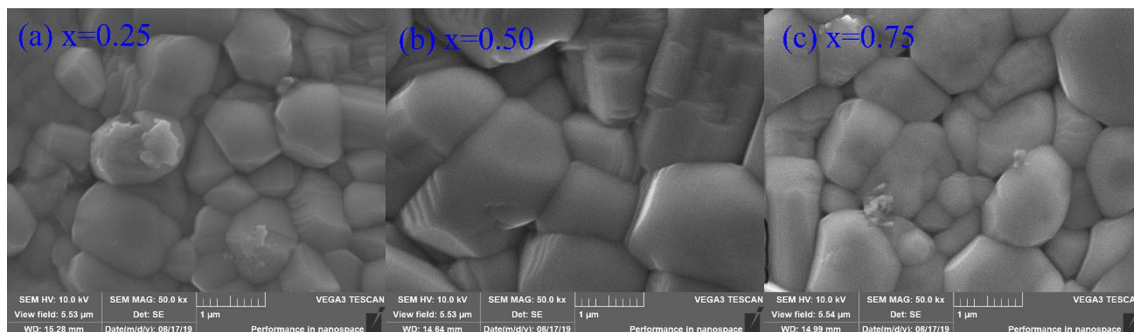


Fig. 2 The microstructures of $(\text{Ca}_{0.28}\text{Ba}_{0.72})_x(\text{Sr}_{0.61}\text{Ba}_{0.39})_{1-x}\text{Nb}_2\text{O}_6$ ($x = 0.25, 0.5, \text{ and } 0.75$) ceramics

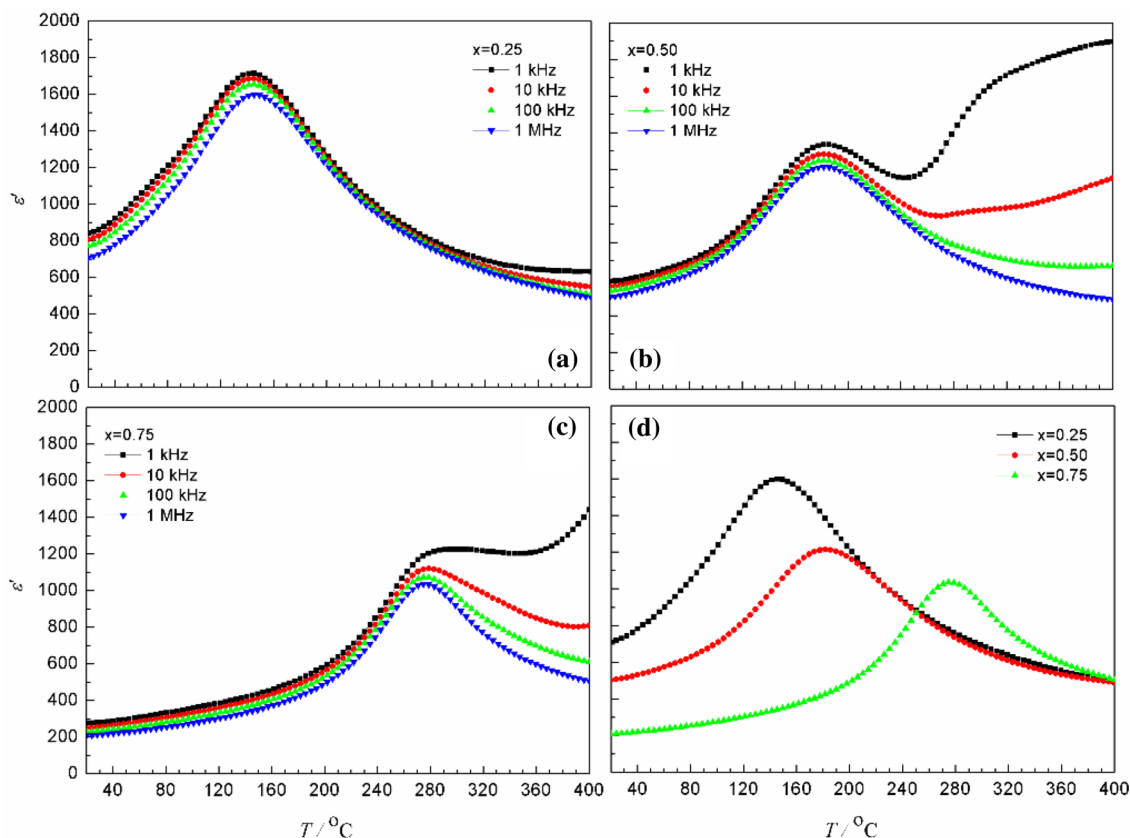


Fig. 3 The temperature-dependent dielectric permittivity of $(\text{Ca}_{0.28}\text{Ba}_{0.72})_x(\text{Sr}_{0.61}\text{Ba}_{0.39})_{1-x}\text{Nb}_2\text{O}_6$ ($x=0.25, 0.5,$ and 0.75) ceramics at 1 kHz–1 MHz (a–c); **d** is a comparison of the dielectric behavior at 1 MHz for all three compositions

of 1 kHz increases significantly at temperatures higher than T_m for CSBN50 and CSBN75. This is defect-induced space charge dielectric relaxation [20]. The phenomenon is consistent with the result of microstructures of ceramics which suggested more defects induced in CSBN50. Although the dielectric permittivity can be fitted by the power law, it was impossible to fit with the Vogel–Fulcher law [21, 22], probably because of a relatively weak polarization fluctuation of the isolated clusters in the system.

To investigate the origin of the variation of the phase transition type, the crystal structures of the ceramics were studied by X-ray diffraction. The XRD diffraction patterns confirmed the P4bm space group for all compositions, and no other impurity phase was observed. Then, the crystal structures were refined based on the Rietveld method [23] with JANA2006 [24]. During structure refinement, Ba^{2+} is fixed at A2 sites [3] while Ca^{2+} is fixed at A1 sites [25] according to the previous results. Sr^{2+} is free to occupy either A1 or A2 position. The Rietveld refinement results are presented in Fig. 4. The successful refinement is confirmed by the very small difference between the measured and refined intensities as shown in Fig. 7 and the low R-factors listed in Table 1.

According to the refined lattice parameters, as shown in Table 1, the lattice parameter is plotted in Fig. 5a. With the increase of x , the lattice parameter a increases while the lattice parameter c decreases. As shown in Fig. 1, the lattice parameter a is mainly decided by A1–O distances. Thus, the decrease of the lattice parameter a indicates that more A1 sites are occupied by the smaller cations. This is evidenced by the site occupancy as listed in Table 2. It indicates that more A1 sites are occupied by the small cation Ca^{2+} with the increase of x .

Using the refined atomic occupancy as listed in Table 2, the site-occupancy factors (s. o. f.) of Ca^{2+} and Sr^{2+} at A1/A2 sites are calculated and plotted in Fig. 5b. Site occupancy factors are defined as:

$$s.o.f._i = \frac{M_i N}{Z} \tag{2}$$

where M_i is the number of atoms per formula unit on site i , N is the number of formula units per unit cell, and Z the number of symmetry-equivalent sites in the unit cell. As shown in the figure, with the increase of x , more A1 sites are occupied by smaller cations (Ca^{2+} and Sr^{2+}) than A2 sites.

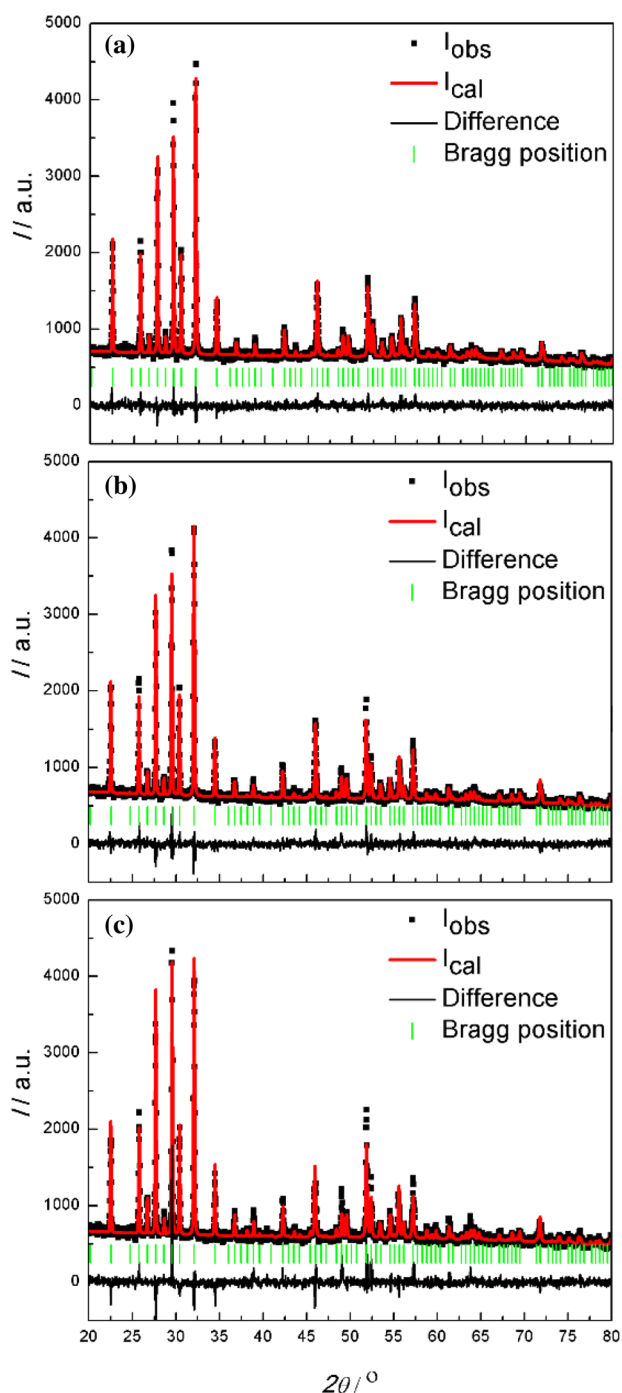


Fig. 4 Rietveld refinement results for $x=0.25$ (a), $x=0.5$ (b), and $x=0.75$ (c) of $(\text{Ca}_{0.28}\text{Ba}_{0.72})_x(\text{Sr}_{0.61}\text{Ba}_{0.39})_{1-x}\text{Nb}_2\text{O}_6$. The dots represent the measured intensities and the lines are the refined intensities. The difference between the measured data and refined data is shown at the bottom. The short vertical lines represent the corresponding Bragg diffraction positions

In other words, A2 sites are more occupied only by Ba^{2+} . In $(\text{Sr}_{1-y}\text{Ba}_y)\text{Nb}_2\text{O}_6$, the material varies from the relaxor to the normal ferroelectrics with the increase of the content of

Table 1 Refined structural parameters and reliability factors for $(\text{Ca}_{0.28}\text{Ba}_{0.72})_x(\text{Sr}_{0.61}\text{Ba}_{0.39})_{1-x}\text{Nb}_2\text{O}_6$ ($x=0.25, 0.5$, and 0.75)

x	0.25	0.50	0.75
$a/\text{Å}$	12.45681	12.45681	12.45681
$c/\text{Å}$	3.94083	3.94083	3.94083
R_p	3.47	3.73	4.76
R_{wp}	4.41	4.82	6.63
GOF	1.18	1.26	1.71

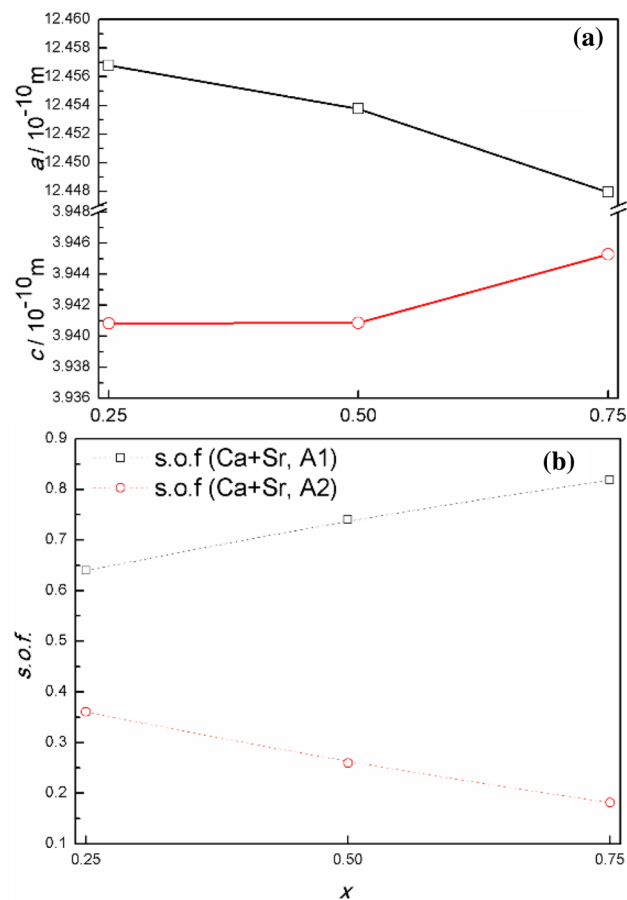


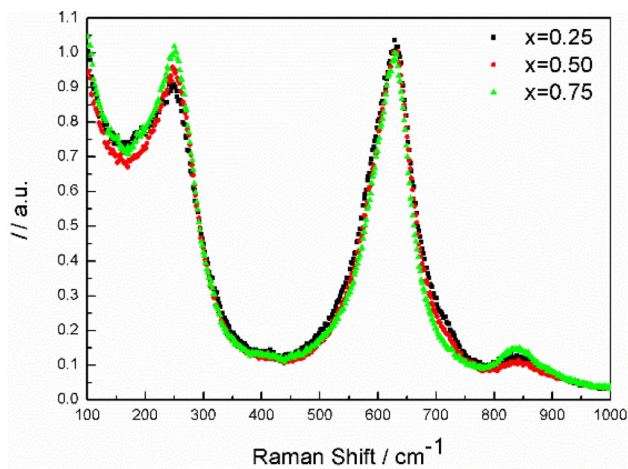
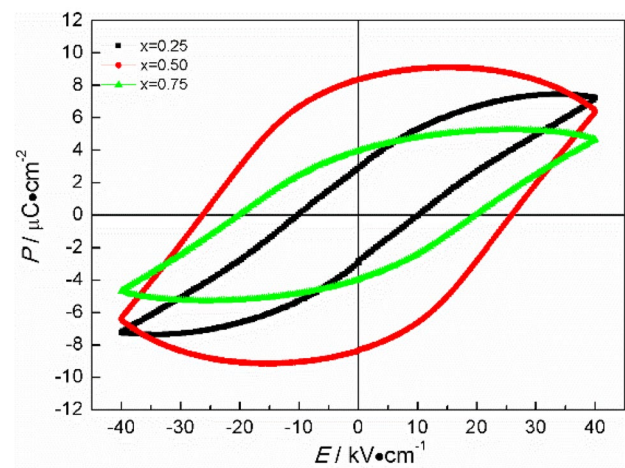
Fig. 5 The refined lattice parameters and the site-occupancy factors of Ca^{2+} and Sr^{2+} at A1 sites and A2 sites in $(\text{Ca}_{0.28}\text{Ba}_{0.72})_x(\text{Sr}_{0.61}\text{Ba}_{0.39})_{1-x}\text{Nb}_2\text{O}_6$ ($x=0.25, 0.5$, and 0.75)

Ba^{2+} . It should be noted that Ba^{2+} occupies only A2 sites [3]. Thus, more A2 sites are occupied by a single cation making TTB a normal ferroelectric, while more A2 sites are occupied by multiple cations making it a relaxor.

To have a better understanding of the improved phase transition temperature, the local structures of the materials have been investigated by Raman spectroscopy and results are plotted in Fig. 6. The data are presented with the normalized intensities by dividing the peak intensities of ~ 630

Table 2 The atomic parameters of $(\text{Ca}_{0.28}\text{Ba}_{0.72})_x(\text{Sr}_{0.61}\text{Ba}_{0.39})_{1-x}\text{Nb}_2\text{O}_6$ ($x=0.25, 0.5, \text{ and } 0.75$)

x	Atom	x/a	x/b	x/c	Occupy	Position
0.25	Ba	0.173550	0.673550	0.495198	0.295312	A2
	Sr (1)	0	0	0.470601	0.139106	A1
	Sr (2)	0.173550	0.673550	0.495198	0.146832	A2
	Ca	0	0	0.470601	0.043750	A1
0.50	Ba	0.173762	0.673762	0.514744	0.346875	A2
	Sr (1)	0	0	0.433787	0.118529	A1
	Sr (2)	0.173762	0.673762	0.514744	0.072097	A2
	Ca	0	0	0.433787	0.087500	A1
0.75	Ba	0.174552	0.674552	0.515523	0.398438	A2
	Sr (1)	0	0	0.431856	0.069144	A1
	Sr (2)	0.174552	0.674552	0.515523	0.026146	A2
	Ca	0	0	0.431856	0.131200	A1

**Fig. 6** Raman spectra of $(\text{Ca}_{0.28}\text{Ba}_{0.72})_x(\text{Sr}_{0.61}\text{Ba}_{0.39})_{1-x}\text{Nb}_2\text{O}_6$ ($x=0.25, 0.5, \text{ and } 0.75$) ceramics**Fig. 7** The polarization–electric field relation of $(\text{Ca}_{0.28}\text{Ba}_{0.72})_x(\text{Sr}_{0.61}\text{Ba}_{0.39})_{1-x}\text{Nb}_2\text{O}_6$ ($x=0.25, 0.5, \text{ and } 0.75$) ceramics

cm. There are two strong peaks around 250/cm and 630/cm, which are related to ionic motions parallel to the polarization direction [26]. The full width at half maximum around 630/cm is thinner, and the peak intensity around 250/cm is higher for $x=0.75$, indicating enhanced ionic motions along the polarization direction. The 840/cm mode is related to the deformation of BO_6 [27], which is also enhanced for CSBN75, indicating the enlarged tilting. Both deformations of oxygen octahedral could be the reason for the improved phase transition temperature with the increase of x . It should be noted that in perovskite that the phase transition is also sensitive to the oxygen octahedral deformation [28].

The polarization–electric field relation of the ceramics is plotted in Fig. 7. The polarization is $7.4\mu\text{C}/\text{cm}^2$, $6.4\mu\text{C}/\text{cm}^2$, and $4.6\mu\text{C}/\text{cm}^2$; the coercive field is 10 kV/cm, 20 kV/cm, 25 kV/cm; the remnant polarization is $3\mu\text{C}/\text{cm}^2$, $8\mu\text{C}/\text{cm}^2$, and $4\mu\text{C}/\text{cm}^2$ for CSBN25, CSBN50, and CSBN75, respectively.

The abnormal large remnant polarization of CSBN50 could be related to more defects induced during sintering as discussed. The polarization values of the ceramics are similar to that of other TTB ceramics, and the hysteresis loops are more “ferroelectric” in comparison with that of $(\text{Ca},\text{Ba})\text{Nb}_2\text{O}_6$ ceramics [17] and are similar to that of $(\text{Sr}_{0.25}\text{Ba}_{0.75})\text{Nb}_2\text{O}_6$ ceramic [3]. With the increase of x , the hysteresis loop varies from a slim shape to a normal shape, which is consistent with the results of dielectric measurement results since the system varies from a relaxor to a normal ferroelectric.

4 Conclusions

The $(\text{Ca}_{0.28}\text{Ba}_{0.72})_x(\text{Sr}_{0.61}\text{Ba}_{0.39})_{1-x}\text{Nb}_2\text{O}_6$ ($x=0.25, 0.5,$ and 0.75) ceramics have been successfully prepared by the solid reaction method. With the increase of x , the phase transition temperature increases gradually, the diffuse phase transition changes to the normal ferroelectric phase transition. These characters make the system have potential applications in high-temperature electronic devices. The origin of the phase transition type is directly related to more A2 sites occupied by Ba^{2+} . The increased phase transition temperature is related to the enhanced ionic motions along the polarization direction and the enlarged tilting of the oxygen octahedron.

Acknowledgments The work is supported by the National Natural Science Foundation of China (Grant no. 11704242) and the Natural Science Foundation of Shanghai, China (Grant no. 17ZR1447200).

References

1. M. Glass, *J. Appl. Phys.* **40**, 4699 (1969)
2. R.R. Neurgaonkar, W.F. Hall, J.R. Oliver, W.W. Ho, W.K. Cory, *Ferroelectrics* **87**, 167 (1988)
3. J. Huang, K. Li, X.Q. Liu, X.L. Zhu, X.M. Chen, *J. Am. Ceram. Soc.* **97**, 507 (2014)
4. S. Wu, C. Sun, Z. Guo, C. Hu, L. Liu, L. Fang, *J. Mater. Sci.* **30**, 17393 (2019)
5. G.H. Olsen, U. Aschauer, N.A. Spaldin, S.M. Selbach, T. Grande, *Phys. Rev. B* **93**, 180101 (2016)
6. J. Dec, W. Kleemann, Th Woike, R. Pankrath, *Eur. Phys. J. B* **14**, 627 (2000)
7. E. Buixaderas, M. Savinov, M. Kempa, S. Veljko, S. Kamba, J. Petzelt, R. Pankrath, S. Kapphan, *J. Phys.* **17**, 653 (2005)
8. M. Eßer, M. Burianek, D. Klamm, M. Mühlberg, *J. Cryst. Growth* **240**, 1 (2002)
9. O.V. Malyschkina, V.S. Lisitsin, J. Dec, T. Łukasiewicz, *Phys. Solid State* **56**, 1824 (2014)
10. S. Pandey, J. Schreuer, M. Burianek, M. Mühlberg, *Phys. Rev. B* **84**, 174102 (2011)
11. Y.J. Qi, C.J. Lu, J. Zhu, X.B. Chen, H.L. Song, H.J. Zhang, X.G. Xu, *Appl. Phys. Lett.* **87**, 082904 (2005)
12. H. Song, H. Zhang, X. Xu, X. Hu, X. Cheng, J. Wang, M. Jiang, *Mater. Res. Bull.* **40**, 643 (2005)
13. H. Liu, X. Yang, *Ferroelectrics* **500**, 310 (2016)
14. H. Liu, X. Yang, *Ferroelectrics* **507**, 69 (2017)
15. L. Li, H. Liu, G. Wen, G. Liu, *Ceram. Int.* **44**, S69 (2018)
16. O. Malyschkina, A. Ivanova, Y. Malyskin, A. Folomeeva, M. Shashkov, J. Dec, *Ferroelectrics* **511**, 76 (2017)
17. S. Ke, H. Fan, H. Huang, H.L.W. Chan, S. Yu, *J. Appl. Phys.* **104**, 024101 (2008)
18. R. Clarke, J.C. Burfoot, *Ferroelectrics* **8**, 505 (1974)
19. K. Uchino, S. Nomura, *Ferroelectrics* **44**, 55 (1982)
20. O. Bidault, P. Goux, M. Kchikech, M. Belkaoui, M. Maglione, *Phys. Rev. B* **49**, 7868 (1994)
21. D. Viehland, S.J. Jang, L.E. Cross, M. Wuttig, *J. Appl. Phys.* **68**, 2916 (1990)
22. D. Viehland, J.F. Li, S.J. Jang, L.E. Cross, M. Wuttig, *Phys. Rev. B* **43**, 8316 (1991)
23. H.M. Rietveld, *J. Appl. Crystallogr.* **2**, 65 (1969)
24. V. Petricek, M. Dusek, L. Palatinus, *Z. Kristallogr.* **229**, 345 (2014)
25. M. Muehlberg, M. Burianek, B. Joschko, D. Klamm, A. Danilewsky, M. Gelissen, L. Bayarjargal, G.P. Görlner, B.O. Hildmann, *J. Cryst. Growth* **310**, 2288 (2008)
26. A. Speghini, M. Bettinelli, U. Caldiño, M.O. Ramírez, D. Jaque, L.E. Bausá, J.G. Solé, *J. Phys. D* **39**, 4930 (2006)
27. J.J. Lima-Silva, D. Garcia, J.M. Filho, J.A. Eiras, A.P. Ayala, *Physica Status Solidi* **241**, 2001 (2004)
28. H. Liu, *J. Am. Ceram. Soc.* **101**, 5281 (2018)

Publisher's Note Springer Nature remains neutral with regard to jurisdictional claims in published maps and institutional affiliations.